One-Way Localized Adiabatic Passage in an Acoustic System

Ya-Xi Shen,[1,*] Yu-Gui Peng,[1,*] De-Gang Zhao,[1] Xin-Cheng Chen,[1] Jie Zhu,[2,3,†] and Xue-Feng Zhu[1,‡]
[1]School of Physics and Innovation Institute, Huazhong University of Science and Technology, Wuhan, 430074, People's Republic of China
[2]Department of Mechanical Engineering, The Hong Kong Polytechnic University, Hung Hom, Kowloon, Hong Kong SAR, People's Republic of China
[3]The Hong Kong Polytechnic University Shenzhen Research Institute, Shenzhen, 518057, People's Republic of China

(Received 6 September 2018; published 8 March 2019)

Stimulated adiabatic passage utilizes radiation pulses to efficiently and selectively transfer population between quantum states, via an intermediate state that is normally decaying. In this Letter, we propose the analog of stimulated adiabatic passage in an acoustic system. It is realized with cavities that correlate through adiabatically time-varying couplings, where the cavities and time-varying couplings mimic discrete states and radiation pulses, respectively. With appropriate arrangements of coupling actions, an acoustic wave can be efficiently transferred from the initial excited cavity to the target cavity in the forward direction, immune to the intermediate dark cavity. On the other hand, for the backward propagation, the acoustic energy is perfectly localized in the intermediate dark cavity and completely dissipated. We analytically, numerically, and experimentally demonstrate such unidirectional sound localization and unveil the essential role of zero-eigenvalue eigenstates in the adiabatic passage process.

DOI: 10.1103/PhysRevLett.122.094501

In 1990, Gaubatz *et al.* [1] experimentally presented the technique of stimulated Raman adiabatic passage through well-tuned radiative interactions. Selective and efficient population transfer was enabled between two different quantum states via a radiative decaying intermediate state without suffering loss [1–10]. Since then, it has spawned a wide range of applications in atomic and molecular physics [11–14], quantum information [15–17], and solid-state physics [18–20]. Recently, this technique has started to impact classical physics, including optical polarization control and frequency conversion [21–24], thanks to the recently proposed quantum-classical analogs, which provide easy-to-implement classical physics platforms for testing various novel physics predicted in quantum systems, such as, to name a few, the Bloch oscillation [25,26], the Zener tunneling [27,28], parity-time symmetric potentials [29–32], and topological insulators [33–36].

Here we present the physical model of stimulated adiabatic passage in an acoustic system. We start from a three-level quantum system ($|1\rangle - |2\rangle - |3\rangle$). The schematic of the three-level system and laser pulses interactions is shown in Figs. 1(a) and 1(b). In this system, the complete transfer of population from an initially populated state $|1\rangle$ to state $|3\rangle$ or, conversely, from state $|3\rangle$ to an intermediate state $|2\rangle$ other than state $|1\rangle$ is enabled via the technique of stimulated adiabatic passage, namely, the adiabatic actions of P (pump) and S (Stokes) lasers in well arrangements [see Fig. 1(b)] [7,10]. Correspondingly, our analog in an acoustic system is proposed with a one-dimensional (1D) cavity chain (A-B-C). The neighboring cavities connected through adiabatically time-varying coupling channels. Here the cavities and time-varying coupling actions play the roles of discrete states and laser pulses in the three-level quantum system, respectively, as presented in Figs. 1(c) and 1(d). It is expected that, with the adiabatic actions of well-arranged intercavity couplings (A–B and B–C), acoustic energy can be totally transferred from cavity A–C in the forward direction without suffering loss from the possibly leaky cavity B. On the other hand, for

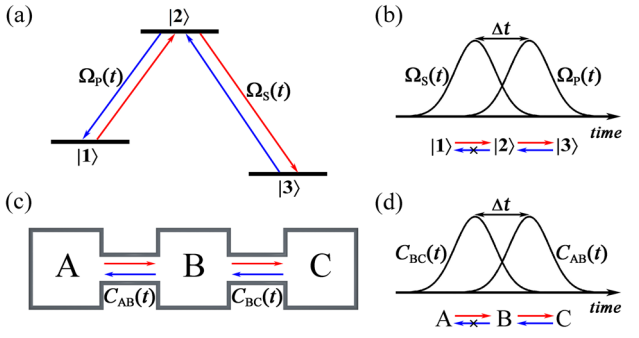

FIG. 1. (a) The three-level quantum system driven by the P (pump) and S (Stokes) lasers. The pump field $\Omega_P(t)$ couples states $|1\rangle$ and $|2\rangle$, while the Stokes field $\Omega_S(t)$ couples states $|2\rangle$ and $|3\rangle$. (b) The counterintuitive pulse sequence where the Gaussian Stokes field $\Omega_S(t)$ is acted before the pump field $\Omega_P(t)$. (c) The schematic of an acoustic cavity chain system. Cavities A and B and B and C are, respectively, connected by the time-varying couplers with the coupling coefficients being $C_{AB}(t)$ and $C_{BC}(t)$. (d) The counter-intuitive coupling sequence where the time-varying coupling $C_{BC}(t)$ is acted before the one of $C_{AB}(t)$.

the backward propagation, the energy coming from cavity C is localized in cavity B and completely dissipated. Very different from previous works on studying acoustic wave localization in reciprocal patterns (e.g., Anderson localization) [37–40], this Letter combines the wave localization and nonreciprocity in adiabatically time-varying acoustic systems. One-way sound localization is demonstrated, which shows promise in versatile important applications, such as single-pass acoustic communication, one-way sound absorption, and unidirectional matching layers.

It is, however, quite challenging to experimentally verify such effect, especially for the part of implementing adiabatically time-varying acoustic coupling channels. By mapping the time dimension into an orthogonal space dimension, we propose to transform the 1D slowly time-varying problem into a 2D static problem and overcome this obstacle, providing a simple and efficient solution to qualitatively extract the field evolution in a three-body interaction system. In this sense, our proposal provides a very unique platform to demonstrate one-way localized adiabatic passage process.

For the acoustic cavity chain system, the adiabatic evolution of sound can be well described by a Schrödinger-type equation as a result of the slowly varying couplings [41]

$$i\frac{d}{dt}\psi(t) = H(t)\psi(t), \tag{1}$$

where $\psi(t)$ denotes the transient state function at time t and $H(t)$ denotes the time-dependent Hamiltonian of the system. The state function $\psi(t)$ can be mapped into the coordinate space (φ_{A}, φ_{B}, φ_{C}) and expressed as $\psi(t) = a(t)\varphi_A + b(t)\varphi_B + c(t)\varphi_C$. The sound intensities in cavities A, B, and C at time t are given by $|a(t)|^2$, $|b(t)|^2$, and $|c(t)|^2$, respectively. Because of the dynamic coupling nature, the Hamiltonian $H(t)$ of the whole system can be written in the matrix form of

$$H(t) = \begin{pmatrix} 0 & C_{AB}(t) & 0 \\ C_{AB}(t) & 0 & C_{BC}(t) \\ 0 & C_{BC}(t) & 0 \end{pmatrix}, \tag{2}$$

where $C_{AB}(t)$ and $C_{BC}(t)$ are the time-varying coupling coefficients between the cavities A and B and B and C. For simplicity, it is assumed that all cavities are identical and lossless; therefore, all the diagonal elements are zero. For the loss case, please refer to Supplemental Material Note 1 [42–44], where the main conclusions of this Letter do not change. For the lossless case, the eigenvalues of the Hamiltonian $H(t)$ are

$$\varepsilon_+ = \sqrt{C_{AB}^2(t) + C_{BC}^2(t)}, \tag{3a}$$

$$\varepsilon_0 = 0, \tag{3b}$$

$$\varepsilon_- = -\sqrt{C_{AB}^2(t) + C_{BC}^2(t)}. \tag{3c}$$

The corresponding eigenvectors are

$$\psi_+(t) = \frac{\sin\theta(t)}{\sqrt{2}}\varphi_A + \frac{1}{\sqrt{2}}\varphi_B + \frac{\cos\theta(t)}{\sqrt{2}}\varphi_C, \tag{4a}$$

$$\psi_0(t) = \cos\theta(t)\varphi_A - \sin\theta(t)\varphi_C, \tag{4b}$$

$$\psi_-(t) = \frac{\sin\theta(t)}{\sqrt{2}}\varphi_A - \frac{1}{\sqrt{2}}\varphi_B + \frac{\cos\theta(t)}{\sqrt{2}}\varphi_C, \tag{4c}$$

where the parameter $\theta(t) = \arctan[C_{AB}(t)/C_{BC}(t)]$. The state function $\psi(t)$ can also be mapped into the eigenvector space (ψ_+, ψ_0, ψ_-), and thus is expressed into [41]

$$\begin{aligned}\psi(t) &= \sum_n \tilde{a}_n(t)\psi_n(t) \\ &= \sum_n a_n(t)\exp\left[-i\int_0^t \varepsilon_n(t')dt'\right]\psi_n(t),\end{aligned} \tag{5}$$

where $n = +, 0, -$, and $\tilde{a}_n(t) = a_n(t)\exp[-i\int_0^t \varepsilon_n(t')dt']$. When the starting point along the time axis is set at t_0, we will obtain an alternative form of

$$\tilde{a}_n(t) = a_n(t_0)\exp\left\{-i\int_{t_0}^t [\varepsilon_n(t') - i\psi_n^*(t')\dot{\psi}_n(t')]dt'\right\}, \tag{6}$$

with the detailed derivations in Supplemental Material Note 2 [44], where $\dot{\psi}(t)$ is the temporal derivative of $\psi(t)$, and $a_n(t_0)$ is determined by the initial condition. For example, an initial condition of $\psi(t_0) = \varphi_{\mathrm{A}}$ means $a_0(t_0) = 1$ and $a_+(t_0) = a_-(t_0) = 0$. In this case, the state function $\psi(t)$ follows the adiabatic evolution of $\psi_0(t)$. From Eq. (4b), the sound intensities in cavities A, B, and C at time t are given by

$$I_A(t) = |\cos\theta(t)|^2, \qquad I_B(t) = 0, \qquad I_C(t) = |\sin\theta(t)|^2. \tag{7}$$

Since the coupling action $C_{BC}(t)$ precedes $C_{AB}(t)$, we have $C_{AB}(t)/C_{BC}(t) \overset{t\to t_0}{\to} 0$ and $C_{AB}(t)/C_{BC}(t) \overset{t\to+\infty}{\to} +\infty$. Because $\theta(t) = \arctan[C_{AB}(t)/C_{BC}(t)]$, the parameter $\theta(t)$ varies from 0 to $\pi/2$ when t changes from t_0 to $+\infty$. From Eq. (7), we obtain that the sound energy transits from cavity A to an intermediate superposition in cavities A and C, and in the end is completely transferred to cavity C. Here cavity B does not get involved in the adiabatic passage process with $I_B(t) = 0$, unveiling the existence of a dark state. Thus, intuitively, the adiabatic passage described by Eq. (7) is independent from cavity B, even if it is lossy.

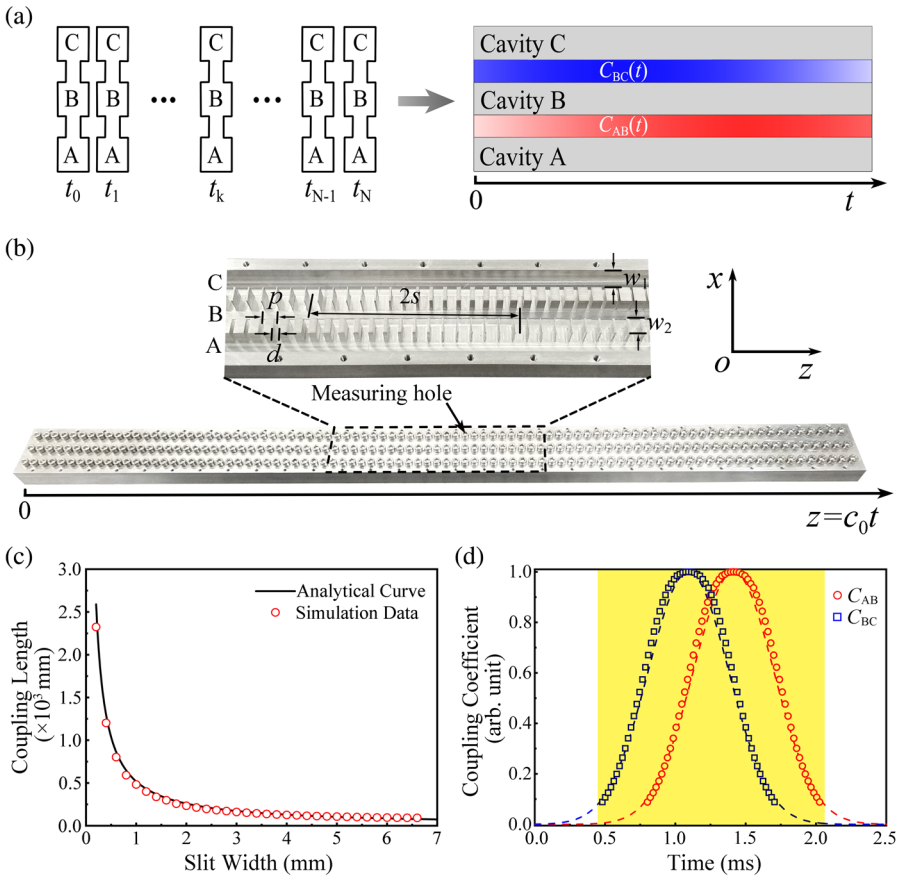

FIG. 2. (a) The schematic of time-varying coupling process among cavities A, B, C. (b) Photograph of the coupled waveguide complex. A mapping between the time dimension (t axis) and an orthogonal space dimension (z axis) is established, that is, $z = c_0 t$. c_0 is the speed of sound. Here the waveguides A, B, C correspond to the cavities A, B, C in Fig. 1(c), respectively. (c) The relation between the coupling length and the slit width. (d) The Gaussian curves of the coupling coefficients between neighboring waveguides. The operation frequency is 8.8 kHz.

If a different initial condition of $\psi(t_0) = \varphi_C$ is given, we have $a_0(t_0) = 0$ and $a_+(t_0) = a_-(t_0) = \sqrt{2}/2$ from Eqs. (4) and (5). In the adiabatic limit, the evolution of the state function is along the eigenstates $\psi_+(t)$ and $\psi_-(t)$ with $\psi_n^*(t)\dot{\psi}_n(t) = 0$, so that from Eq. (6) we obtain the amplitudes $\tilde{a}_+(t) = \tilde{a}_-^*(t) = e^{-i\beta(t)}/\sqrt{2}$, where the phase $\beta(t)$ is

$$\beta(t) = \int_{t_0}^{t} \varepsilon_+(t')dt'. \tag{8}$$

With Eqs. (4)–(6), we can derive the sound intensities in cavities A, B, and C for the different initial condition at time t

$$I_A(t) = |\sin\theta(t)|^2 |\cos\beta(t)|^2, \qquad I_B(t) = |\sin\beta(t)|^2,$$
$$I_C(t) = |\cos\theta(t)|^2 |\cos\beta(t)|^2. \tag{9}$$

Under the same coupling action $\theta(t) = 0 \to \pi/2$ and with the phase set as $\beta(t) = 0 \to (2k+1)\pi/2$ (k is an integer) from $t = t_0$ to $t = +\infty$, we obtain that the sound energy transits from cavity C to an oscillatory superposition in cavities A, B, and C and eventually is completely transferred to cavity B. In this case, all energy will be dissipated if cavity B is lossy. The aforementioned analysis shows that the acoustic version of the stimulated adiabatic passage is featured with unidirectional wave localization, that is, $A \to C$ and $C \to B \not\to A$, when the coupling actions are well designed.

Figure 2(a) vividly displays the time-varying coupling process of cavities A, B, and C in terms of the limit idea. However, straightforward experimental implementations of the adiabatically time-varying coupling channels with well-designed coupling strengths are quite challenging. Instead, we map the time dimension (t axis) into an orthogonal space dimension (z axis), where the Doppler effect can be ignored in the adiabatic processes [33,36]. Here we propose a coupled waveguide comprising three parallel air pipes connected by equally spaced slits of varied widths (p is a constant), as shown in Fig. 2(b). It provides a static platform to demonstrate the stimulated adiabatic passage of sound. The z dimension is regarded as a pseudotime dimension. For each waveguide, there are 87 perforated holes equally spaced by 10 mm for inside field measurement [49]. The sample is made of an aluminum

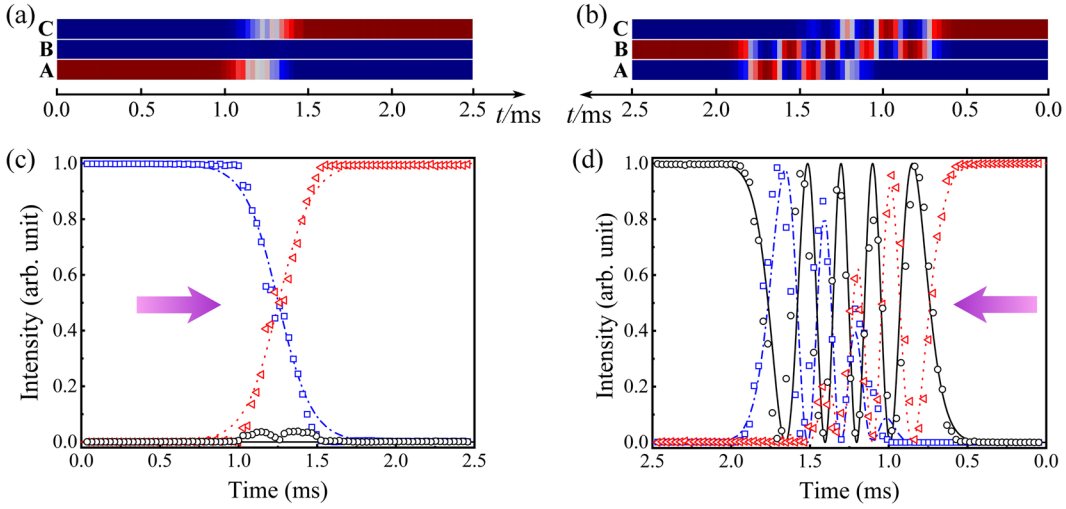

FIG. 3. Experimental characterization of the one-way localized adiabatic passage process. (a),(b) The measured evolutions of normalized sound intensities when the sound waves are launched from cavity A and cavity C, respectively. (c),(d) The measured sound intensities at the different times in cavities A, B, and C (namely, the sound intensities extracted at different locations along the waveguides A, B, and C) when the sound waves are launched from cavity A and cavity C. Here the blue squares (blue dash-dotted line), black circles (black solid line), and red triangles (red dotted line) correspond to the measured (analytical) data in cavities A, B, and C. The analytical curves in (c),(d) are calculated by Eqs. (7) and (9), respectively. The operation frequency is 8.8 kHz.

alloy, which is rigid with respect to air due to the large impedance mismatch. The structural parameters are marked in Fig. 2(b), where the width of air pipes is $w_1 = 10$ mm, the thickness between adjacent air pipes $w_2 = 8$ mm, the distance between the equally spaced slits $p = 7$ mm, and the delayed distance between two coupling actions $\Delta z = 2s = 110$ mm (corresponding to the time delay of 0.32 ms).

From the above analysis and Supplemental Material Note 1 [44], the state function $\psi(t)$ of the acoustic waveguide chain system does not change, no matter whether the cavity B is lossless or lossy, due to the existence of a dark state. The only factor to affect the acoustic adiabatic passage process is the adiabatic limit condition, that is [5,8,42],

$$|\varepsilon_{\pm} - \varepsilon_0| \gg |\psi_{\pm}(t)\dot{\psi}_0(t)|, \tag{10}$$

for which the rigorous analysis is appended in Supplemental Material Note 3 [44]. In order to fulfill the adiabatic limit condition, we introduce two z-dependent Gaussian-shaped coupling coefficients between neighboring waveguides, which can be equivalently regarded as time-dependent Gaussian-shaped coupling coefficients via the mapping $z = c_0 t$. The coupling coefficients $C_{AB}(t)$ and $C_{BC}(t)$ are intuitively related with the width of slits and the operation frequency of sound. Note that we define the coupling coefficients by $C = \pi/L$, where L denotes the coupling length (see Supplemental Material Note 4 [44] for the derivations). In one coupling length, all sound waves will funnel from one waveguide to the neighboring waveguide and then back to the original waveguide. In Fig. 2(c), we plot the relation between the coupling length L and the slit width d at the operation frequency of 8.8 kHz, which is derived from the numerical simulations. The result shows that the relation curve can be well fitted by a function of $L = a/d$, where a is chosen to be 518 mm^2. Assuming the Gaussian-shaped slit width distribution satisfies $d = d_0 e^{-c_0^2 t^2/\sigma^2}$, we can eventually derive the time-dependent coefficients $C_{AB}(t) = (\pi d_0/a) e^{-[(c_0 t - z_0) - s]^2/\sigma^2}$ and $C_{BC}(t) = (\pi d_0/a) e^{-[(c_0 t - z_0) + s]^2/\sigma^2}$, as shown in Fig. 2(d), where the parameters $\sigma = 127$, $d_0 = 6.5$, and $z_0 = 430$ mm. In experiments, there exist fabrication limits that the slit width and the slit spacing cannot be infinitely small. For cutting straight slits of the depth 10 mm, the slit width can hardly be smaller than 0.4 mm for the machine tool. Therefore, the coupling length is limited to be less than 1102.2 mm (coupling coefficient $C > 2.84 \times 10^{-3}$ mm^{-1}), as reflected by the fitted curve in Fig. 2(c) and Supplemental Material Table 1 [44]. The normalized coupling coefficient ($C/C_{\max}$) used in experiments thus has a cutoff at 0.088, as shown by the square and circle dots in Fig. 2(d).

In the experiment, the evolution of sound intensity field in the coupled cavity system is acquired by measurements in the perforated holes on the waveguide sample [Fig. 2(b)]. The operation frequency is 8.8 kHz. For the designed sample, considering the whole evolution happens from 0 to 2.5 ms, we have $\theta(t) = 0 \to \pi/2$ and the phase $\beta(t) = 0 \to 9\pi/2$, as calculated in Supplemental Material Note 5 [44]. Therefore, based on Eqs. (7) and (9), we obtain two different field evolutions. For the first one, we have $I_A(0) = 1$, $I_B(0) = 0$, and $I_C(0) = 0$ for the initial state and $I_A(2.5) = 0$, $I_B(2.5) = 0$, and $I_C(2.5) = 1$ for the final state. For the other one, we have $I_A(0) = 0$, $I_B(0) = 0$, and $I_C(0) = 1$ for the initial state and $I_A(2.5) = 0$, $I_B(2.5) = 1$, and $I_C(2.5) = 0$ for the final state. As a result, there exists

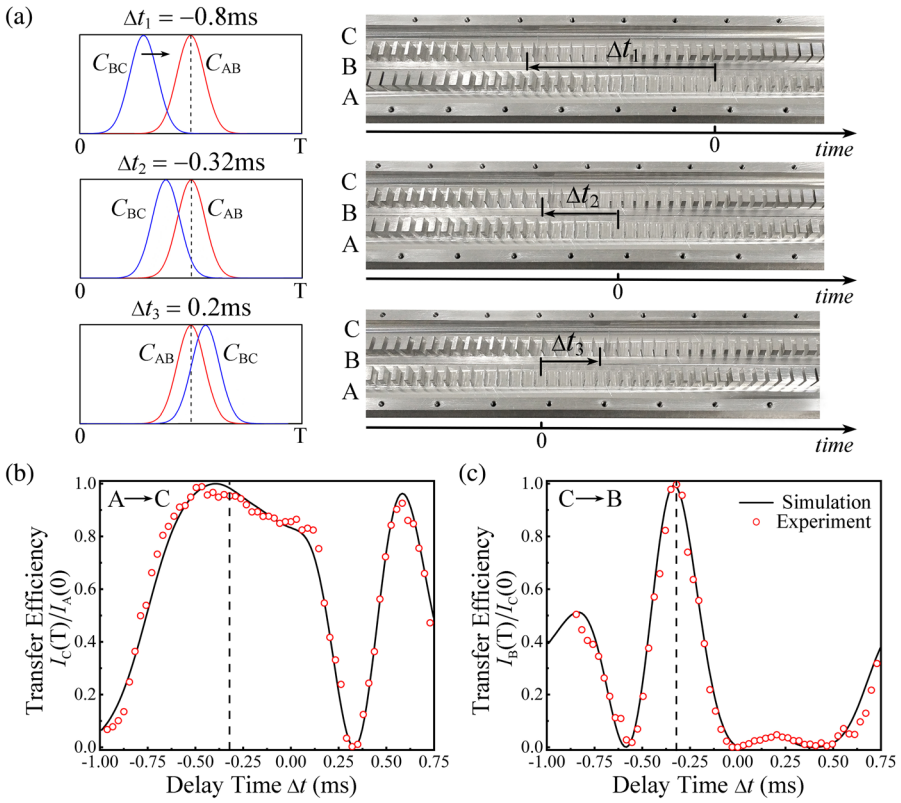

FIG. 4. (a) The coupling actions between neighboring cavities. The delay time between the coupling actions is tailored by sliding the upper part of the waveguide sample with the bottom part fixed, shown by the sample photos. T is the total interaction time between the two coupling actions. (b) Transfer efficiency of $A \to C$ versus the delay time Δt. (c) Transfer efficiency of $C \to B$ versus the delay time Δt. The black solid line and the red circles denote the numerical simulation (see Supplemental Material Note 6 [44] for the procedure) and experimental measurement data, respectively. The operation frequency is 8.8 kHz.

an interesting phenomenon of the unidirectional sound localization, which involves two irreversible transports ($A \to C$ and $C \to B$), undergoing the same adiabatic actions of well-arranged couplings. In Figs. 3(a)–3(d), the measured sound intensity evolutions for different initial conditions agree well with the theoretical prediction. In Figs. 3(a) and 3(c), when sound is launched at cavity A, around 98% of sound energy is transferred to cavity C. If we reversely provide sound input at cavity C in Figs. 3(b) and 3(d), over 98% of total sound energy is localized at the intermediate cavity B instead of getting transferred back to cavity A. It should be mentioned that for the transport $A \to C$, cavity B should always be dark with no sound there, as revealed by the black solid line in Fig. 3(c). However, the measured data in cavity B are not absolutely zero but trivial with the value <4% [see the black circles in Fig. 3(c)], which is attributed to the limitations of coupling coefficient cutoff and finite slit spacing. We can regard cavity B as a dark one [50]. In Supplemental Material Note 6 [44], we attach the details about the integral form of the adiabatic limit condition as well as the numerical simulation of the one-way localized adiabatic passage of sound.

We further investigate the characteristic signature of acoustic adiabatic passage with respect to the delay time between two different coupling actions. In experiments, the delay time Δt between the coupling actions $C_{BC}(t)$ and $C_{AB}(t)$ is modified by sliding one waveguide over the other, as shown in Fig. 4(a). The transfer efficiency of $A \to C$ versus the delay time is plotted in Fig. 4(b). We start from the counterintuitive case, when the coupling $C_{BC}(t)$ precedes $C_{AB}(t)$, namely, $\Delta t < 0$. In the situation where the coupling $C_{BC}(t)$ acts too early, there is nearly no overlap between $C_{BC}(t)$ and $C_{AB}(t)$, as shown by the case of $\Delta t_1 = -0.8$ ms in Fig. 4(a). From the definition of $\theta(t)$ and Eq. (10), we find that the adiabatic limit condition is broken in the evolution process, so the state function cannot follow Eq. (7). As a result, cavity B is no longer dark anymore [see Supplemental Material Note 6 and Fig. S5(a) [44]], the transfer efficiency from cavity A to cavity C is low, as revealed by both simulation and experiment data in Fig. 4(b). When the action $C_{BC}(t)$ approaches toward $C_{AB}(t)$, the adiabatic limit condition becomes fulfilled, and the state function follows Eq. (7) with a dark state formed [$I_B(t) = 0$]. It can be observed that the transfer efficiency $A \to C$ increases dramatically. At the exceptional point of $\Delta t_2 = -0.32$ ms, we have $\theta(2.5) = \pi/2$ and the transfer efficiency hits unitary according to Eq. (7).

When the coupling $C_{BC}(t)$ lags behind $C_{AB}(t)$, namely, intuitive coupling sequence $\Delta t > 0$, we have

$\theta(t) = \pi/2 \to 0$ during the whole evolution. In this case, the state function cannot follow Eq. (7) but rather Eq. (9). Based on Eq. (9), cavity B cannot be dark, so that the transfer efficiency $A \to C$ decreases to a lower level. The transfer efficiency for $C \to A$ is appended in Supplemental Material Note 6 and Fig. S5(b) [44], which clearly shows an irreversible process for sound transition between sites A and C. Figure 4(c) shows the transfer efficiency of $C \to B$ versus the delay time. The state function follows Eq. (9) in the adiabatic condition. Since in our design we have both $\theta(2.5) = \pi/2$ and $\beta(2.5) = 9\pi/2$ at $\Delta t = -0.32$ ms, the transfer efficiency is unitary, as shown by both simulation and experiment in Fig. 4(c). In Supplemental Material Note 7 [44], we further discuss the irreversible adiabatic passage of sound in a multiple-cavities-chain system with the neighboring cavities correlated by well-designed time-varying couplings. We find that only when the number of cavities is odd will there exist a zero-eigenvalue eigenstate (or a dark state) that enables a complete sound transfer from an initially excited cavity to the target cavity [45–48].

In conclusion, we propose and thoroughly investigate the acoustic version of a stimulated adiabatic passage. Through the combined adiabatically pseudotime-varying coupling actions, we show that, in the forward process, sound energy can be directly transferred from an initially excited cavity to the target cavity via a dark state, immune to disturbance from intermediate cavities. Conversely, the sound energy distribution in the cavities becomes oscillatory. With properly tailored couplings, the sound energy can be completely localized in one targeted intermediate cavity. Our study provides an alternative and easy-to-implement platform for investigating on-purpose and robust nonreciprocal wave manipulations in adiabatically time-varying acoustic systems.

This work was supported by National Natural Science Foundation of China (Grants No. 11674119, No. 11774297, No. 11690030, No. 11690032). J. Z. acknowledges the support from the Early Career Scheme (ECS) of Hong Kong RGC (Grant No. PolyU 252081/15E).

*Y. X. S. and Y. G. P. contributed equally to this work.
†To whom correspondence should be addressed.
jiezhu@polyu.edu.hk
‡To whom correspondence should be addressed.
xfzhu@hust.edu.cn

[1] U. Gaubatz, P. Rudecki, S. Schiemann, and K. Bergmann, J. Chem. Phys. **92**, 5363 (1990).
[2] J. R. Kuklinski, U. Gaubatz, F. T. Hioe, and K. Bergmann, Phys. Rev. A **40**, 6741 (1989).
[3] G. Z. He, A. Kuhn, S. Schiemann, and K. Bergmann, J. Opt. Soc. Am. B **7**, 1960 (1990).
[4] B. W. Shore, Contemp. Phys. **36**, 15 (1995).
[5] T. A. Laine and S. Stenholm, Phys. Rev. A **53**, 2501 (1996).
[6] K. Bergmann, H. Theuer, and B. W. Shore, Rev. Mod. Phys. **70**, 1003 (1998).
[7] N. V. Vitanov, T. Halfmann, B. W. Shore, and K. Bergmann, Annu. Rev. Phys. Chem. **52**, 763 (2001).
[8] B. W. Shore, Acta Phys. Slovaca **58**, 243 (2008).
[9] K. Bergmann, N. V. Vitanov, and B. W. Shore, J. Chem. Phys. **142**, 170901 (2015).
[10] N. V. Vitanov, A. A. Rangelov, B. W. Shore, and K. Bergmann, Rev. Mod. Phys. **89**, 015006 (2017).
[11] T. Takekoshi, L. Reichsöllner, A. Schindewolf, J. M. Hutson, C. Ruth Le Sueur, O. Dulieu, F. Ferlaino, R. Grimm, and H.-C. Nägerl, Phys. Rev. Lett. **113**, 205301 (2014).
[12] M. Y. Guo, B. Zhu, B. Lu, X. Ye, F. Wang, R. Vexiau, N. Bouloufa-Maafa, G. Quéméner, O. Dulieu, and D. Wang, Phys. Rev. Lett. **116**, 205303 (2016).
[13] C. L. Webb, R. M. Godun, G. S. Summy, M. K. Oberthaler, P. D. Featonby, C. J. Foot, and K. Burnett, Phys. Rev. A **60**, R1783 (1999).
[14] A. Kuhn, S. Steuerwald, and K. Bergmann, Eur. Phys. J. D **1**, 57 (1998).
[15] X. Lacour, N. Sangouard, S. Guérin, and H. R. Jauslin, Phys. Rev. A **73**, 042321 (2006).
[16] B. Rousseaux, S. Guérin, and N. V. Vitanov, Phys. Rev. A **87**, 032328 (2013).
[17] D. Møller, L. B. Madsen, and K. Mølmer, Phys. Rev. A **77**, 022306 (2008).
[18] D. A. Golter, T. Oo, M. Amezcua, K. A. Stewart, and H. L. Wang, Phys. Rev. Lett. **116**, 143602 (2016).
[19] P. G. Di Stefano, E. Paladino, A. D'Arrigo, and G. Falci, Phys. Rev. B **91**, 224506 (2015).
[20] K. S. Kumar, A. Vepsalainen, S. Danilin, and G. S. Paraoanu, Nat. Commun. **7**, 10628 (2016).
[21] S. Longhi, G. Della Valle, M. Ornigotti, and P. Laporta, Phys. Rev. B **76**, 201101 (2007).
[22] S. Longhi, Phys. Rev. E **73**, 026607 (2006).
[23] E. Dimova, A. Rangelov, and E. Kyoseva, J. Opt. **17**, 075605 (2015).
[24] G. Pora and A. Arie, J. Opt. Soc. Am. B **29**, 2901 (2012).
[25] R. Sapienza, P. Costantino, D. Wiersma, M. Ghulinyan, C. J. Oton, and L. Pavesi, Phys. Rev. Lett. **91**, 263902 (2003).
[26] H. Trompeter, W. Krolikowski, D. N. Neshev, A. S. Desyatnikov, A. A. Sukhorukov, Y. S. Kivshar, T. Pertsch, U. Peschel, and F. Lederer, Phys. Rev. Lett. **96**, 053903 (2006).
[27] M. Ghulinyan, C. J. Oton, Z. Gaburro, L. Pavesi, C. Toninelli, and D. S. Wiersma, Phys. Rev. Lett. **94**, 127401 (2005).
[28] H. Trompeter, T. Pertsch, F. Lederer, D. Michaelis, U. Streppel, A. Bräuer, and U. Peschel, Phys. Rev. Lett. **96**, 023901 (2006).
[29] T. Liu, X. F. Zhu, F. Chen, S. J. Liang, and J. Zhu, Phys. Rev. Lett. **120**, 124502 (2018).
[30] C. Z. Shi, M. Dubois, Y. Chen, L. Cheng, H. Ramezani, Y. Wang, and X. Zhang, Nat. Commun. **7**, 11110 (2016).
[31] R. Fleury, D. Sounas, and A. Alu, Nat. Commun. **6**, 5905 (2015).
[32] X. F. Zhu, H. Ramezani, C. Z. Shi, J. Zhu, and X. Zhang, Phys. Rev. X **4**, 031042 (2014).
[33] M. Xiao, W. J. Chen, W. Y. He, and C. T. Chan, Nat. Phys. **11**, 920 (2015).

[34] Y. G. Peng, C.-Z. Qin, D.-G. Zhao, Y.-X. Shen, X.-Y. Xu, M. Bao, H. Jia, and X.-F. Zhu, Nat. Commun. **7**, 13368 (2016).
[35] C. He, X. Ni, H. Ge, X.-C. Sun, Y.-B. Chen, M.-H. Lu, X.-P. Liu, and Y.-F. Chen, Nat. Phys. **12**, 1124 (2016).
[36] J. Y. Lu, C. Qiu, L. Ye, X. Fan, M. Ke, F. Zhang, and Z. Liu, Nat. Phys. **13**, 369 (2017).
[37] G. Lefebvre *et al.*, Phys. Rev. Lett. **117**, 074301 (2016).
[38] C. Even, S. Russ, V. Repain, P. Pieranski, and B. Sapoval, Phys. Rev. Lett. **83**, 726 (1999).
[39] M. Filoche and S. Mayboroda, Phys. Rev. Lett. **103**, 254301 (2009).
[40] P. W. Anderson, Phys. Rev. Lett. **109**, 1492 (1958).
[41] A. Messiah, *Quantum Mechanics* (North-Holland, Amsterdam) (1962).
[42] B. T. Torosov, G. D. Valle, and S. Longhi, Phys. Rev. A **89**, 063412 (2014).
[43] E. M. Graefe, A. A. Mailybaev, and N. Moiseyev, Phys. Rev. A **88**, 033842 (2013).
[44] See Supplemental Material at http://link.aps.org/supplemental/10.1103/PhysRevLett.122.094501 more details on simulations and experiments, a theoretical analysis of the non-Hermitian systems, and a discussion on multiple-cavities-chain systems, which includes Refs. [5,41–43, 45–48].
[45] N. V. Vitanov, Phys. Rev. A **58**, 2295 (1998).
[46] C. Ciret, V. Coda, A. A. Rangelov, D. N. Neshev, and G. Montemezzani, Phys. Rev. A **87**, 013806 (2013).
[47] F. T. Hioe and C. E. Carroll, Phys. Rev. A **37**, 3000 (1988).
[48] B. W. Shore, K. Bergmann, J. Oreg, and S. Rosenwaks, Phys. Rev. A **44**, 7442 (1991).
[49] Y. X. Shen, Y. G. Peng, X. C. Chen, D. G. Zhao, and X. F. Zhu, Sci. Rep. **7**, 45603 (2017).
[50] M. Mrejen, H. Suchowski, T. Hatakeyama, C. Wu, L. Feng, K. O'Brien, Y. Wang, and X. Zhang, Nat. Commun. **6**, 7565 (2015).